

Spin stiffness of graphene and zigzag graphene nanoribbons

Jun-Won Rhim and Kyungsun Moon

Department of Physics and IPAP, Yonsei University, Seoul 120-749, Korea

(Received 5 August 2009; revised manuscript received 15 September 2009; published 20 October 2009)

We theoretically study the spin stiffness of graphene and graphene nanoribbon based on the Hubbard-type Hamiltonian. Using the Hartree-Fock method with the inclusion of the adiabatic spin twist, we have obtained the effective energy functional and investigated the magnetic excitations of the two-dimensional graphene and zigzag graphene nanoribbon (ZGNR). We have analyzed the spin stiffness of the system with varying temperature and the strength of on-site Coulomb repulsion. For ZGNR, we have also studied the effect of the lateral electric field on the spin stiffness. As the field increases, the spin stiffness decreases and reaches less than the half of the zero-field value. However, we remarkably notice that there exists a critical value of the electric field above which the stiffness starts to increase showing a cusp-like behavior. This critical point is found to coincide exactly with the metal-insulator transition point of ZGNR.

DOI: [10.1103/PhysRevB.80.155441](https://doi.org/10.1103/PhysRevB.80.155441)

PACS number(s): 75.75.+a, 73.22.-f, 73.20.-r

I. INTRODUCTION

Graphene, a monolayer honeycomb sheet of carbon atoms, has attracted a remarkable interest both theoretically and experimentally since it first became available in 2004.¹ This enthusiasm has been created by the facts that it has very peculiar electronic properties and also has great potential as a base material for future nanotechnology devices.^{2,3} Graphene has also attracted much attention as a candidate for an organic ferromagnetic material since the observation of ferromagnetic order in proton-irradiated graphite at ambient temperature.⁴⁻⁶ On the other hand, by reducing dimensionality via cutting graphene and making it into a graphene nanoribbon (GNR), it has been demonstrated that this carbon allotrope can be further qualified as a semiconductor due to the gap opening and may be useful for the spintronics for certain GNR due to the emergence of intrinsic edge magnetism as well.⁷⁻¹¹ Recently the electronic, magnetic, and transport properties of GNRs have been extensively studied¹²⁻²² along with the impressive experimental progress.²³⁻³³ It has been reported that very narrow GNRs with smooth edges can be fabricated by ripping apart carbon nanotubes^{23,24} while some groups have been able to measure edge effects from the electronic and transport properties.^{29,31,32}

It was shown that a zigzag graphene nanoribbon (ZGNR) supports the magnetic edge states which are ferromagnetic along each edge and antiferromagnetic between the two different edges due to the bipartite nature of the lattice structure.^{10,11,34} The first-principles calculations by Son *et al.* which demonstrate that ZGNRs can be changed into half metallic by applying transverse electric field to the system⁹ have fueled much research activities related to spintronics applications of the ZGNR.^{14,17,22} Recently, Yazyev *et al.* calculated that ZGNRs have correlation length of about 1nm at room temperature and it would reach more than micrometer at low temperature (below 10 K).²² This means that ZGNR-spintronics devices can function at low temperatures for nanoscale circuits made of graphitic ribbons. They have noticed that the large spin stiffness of the ZGNR leads to its relatively long spin-correlation length in spite that it has very small magnetic anisotropy. Hence the spin stiffness is one of

the key parameters for the future application of the ZGNR spintronics.

In the present paper, we calculate the spin stiffness of graphene and ZGNR at half filling by solving the Hubbard-type model using the Hartree-Fock approximation. Since one of the issues is the feasibility of the spintronics operation at room temperature, we investigate the spin stiffness of graphene and ZGNR as a function of temperature. In the case of graphene, which is intrinsically nonmagnetic, we assign an unphysically large on-site Coulomb energy to look into the magnetic phase. We have studied the dependence of the spin stiffness of both graphene and ZGNR on the strength of the on-site Coulomb repulsion. Focusing on the ZGNR, while it exhibits half metallicity under the transverse electric field, it is still to be studied whether it has sufficiently large spin stiffness under the electric field. Motivated by this question, we investigate how the laterally applied electric field affects the ZGNR's spin stiffness.

II. SPIN STIFFNESS OF 2D GRAPHENE

In this section, we introduce the Hartree-Fock approximation for the tight-binding Hubbard model and apply this method to obtain the spin stiffness of two-dimensional (2D) graphene. The spin stiffness ρ_s is a crucial parameter in the spin wave theory. It is defined to be the quadratic coefficient of the free-energy increment arising from the adiabatic twist of the order parameter by an angle θ along a certain specific direction.

$$F(\theta) = F(0) + \frac{1}{2}N\rho_s\theta^2 + O(\theta^4). \quad (1)$$

Here, $F(\theta)$ is the free energy and N is the number of the primitive cells. The spin stiffness is also closely related to the spin-wave velocity. According to the hydrodynamic theory of Halperin and Hohenberg, the spin stiffness of the Heisenberg antiferromagnet satisfies a simple relationship $\rho_s = v^2/\chi_\perp$ where v is the spin-wave velocity and χ_\perp is the transverse susceptibility.³⁵ Later, it was proved that the hydrodynamic relation is also valid for the itinerant electron systems such

as Hubbard model.³⁶ We adopt the mean-field approach developed by Denteneer *et al.* with which they calculated the spin stiffness of the square lattice at half filling.³⁷ Their results were shown to be consistent with those from the variational Monte Carlo calculations and the series-expansion method.³⁸

The Hubbard Hamiltonian to describe the graphene system can be written by

$$\mathcal{H} = - \sum_{\langle i,j \rangle, \sigma, \alpha} t_0 c_{i\sigma}^{\alpha\dagger} c_{j\sigma}^{-\alpha} + U \sum_{i,\alpha} n_{i\uparrow\alpha} n_{i\downarrow\alpha}, \quad (2)$$

where i and j denote the nearest neighbors, σ represents the spin index, $\alpha = \pm 1$ is the sublattice index, t_0 is the hopping amplitude, and U is the on-site Coulomb repulsion. Here, we have introduced two kinds of field operators $c_{\sigma}^{+\dagger}$ and $c_{\sigma}^{-\dagger}$ to represent the bipartite lattice structure of graphene.

Allowing the spin-flip processes, the mean-field one-body Hamiltonian obtained by the Hartree-Fock decoupling is given by

$$\begin{aligned} \mathcal{H}_{HF} = & - \sum_{\langle i,j \rangle, \sigma, \alpha} t_0 c_{i\sigma}^{\alpha\dagger} c_{j\sigma}^{-\alpha} + U \sum_{i,\sigma,\alpha} \langle n_{i,-\sigma}^{\alpha} \rangle n_{i\sigma}^{\alpha} - U \sum_{i,\alpha} (\langle S_i^{\alpha-} \rangle S_i^{\alpha+} \\ & + \text{H.c.}) + E_0, \end{aligned} \quad (3)$$

where $S_i^{\alpha+} = c_{i,\uparrow}^{\alpha\dagger} c_{i,\downarrow}^{\alpha}$, $S_i^{\alpha-} = c_{i,\downarrow}^{\alpha\dagger} c_{i,\uparrow}^{\alpha}$, and $E_0 = U \sum_{i,\alpha} (\langle S_i^{\alpha-} \rangle \langle S_i^{\alpha+} \rangle - \langle n_{i,\uparrow}^{\alpha} \rangle \langle n_{i,\downarrow}^{\alpha} \rangle)$.

When U is large enough ($U > 2.3t_0$), the ground configuration of graphene at half filling is known to have a Néel order because of the bipartite nature of graphene.^{34,39} Since the system has $SU(2)$ symmetry, we have chosen a spin configuration with $\langle S_i^{\alpha\alpha} \rangle = \frac{1}{2} (\langle n_{i\uparrow}^{\alpha} \rangle - \langle n_{i\downarrow}^{\alpha} \rangle) = 0$. Based on this ground state spin order, a transverse spin excitations can be generated by using the following ansatz:

$$U \langle S_i^{\alpha-} \rangle = \alpha \Gamma e^{i\vec{q} \cdot \vec{R}_i^{\alpha}} \quad (4)$$

where Γ is a positive constant and \vec{R}_i^{α} denotes the lattice point. Here, the Néel ground state is imposed by the sublattice index $\alpha = \pm 1$. Now, we obtain the Fourier transformed Hartree-Fock Hamiltonian

$$\begin{aligned} \mathcal{H}_{HF} = & - t_0 \sum_{\vec{k}, \sigma} (\phi_{\vec{k}} c_{\vec{k}\sigma}^{+\dagger} c_{\vec{k}\sigma}^{-} + \text{H.c.}) + U \sum_{\vec{k}, \sigma, \alpha} \langle n_{-\sigma}^{\alpha} \rangle n_{\vec{k}\sigma}^{\alpha} \\ & - \Gamma \sum_{\vec{k}, \alpha} \alpha (c_{\vec{k},\uparrow}^{\alpha\dagger} c_{\vec{k}-\vec{q},\downarrow}^{\alpha} + \text{H.c.}) + E_0, \end{aligned} \quad (5)$$

where $\langle n_{\sigma}^{\alpha} \rangle$ can be replaced by $1/2$ at half filling and $\phi_{\vec{k}} = e^{i1/2(k_x\sqrt{3}+k_y)} + e^{-ik_x\sqrt{3}} + e^{i1/2(k_x\sqrt{3}-k_y)}$.

The spin stiffness tensor of graphene can be obtained by collecting the coefficient of the quadratic terms of the free-energy expansion. One can show that the off-diagonal elements of the stiffness tensor vanish and the spin excitations are isotropic so that $F_{HF}(\vec{q}) \approx F_{HF}(0) + \frac{1}{2} N \rho_s q^2$ where the Hartree-Fock free energy is given by $F_{HF} = -\frac{1}{\beta} \ln(\text{Tr} e^{-\beta(\mathcal{H}_{HF} - \mu N)})$ with $\beta = 1/k_B T$. Here μ is the chemical potential and it becomes $U/2$ at half filling where the particle hole symmetry holds. The finite-temperature spin stiffness of graphene at half filling can be calculated by the following formula:

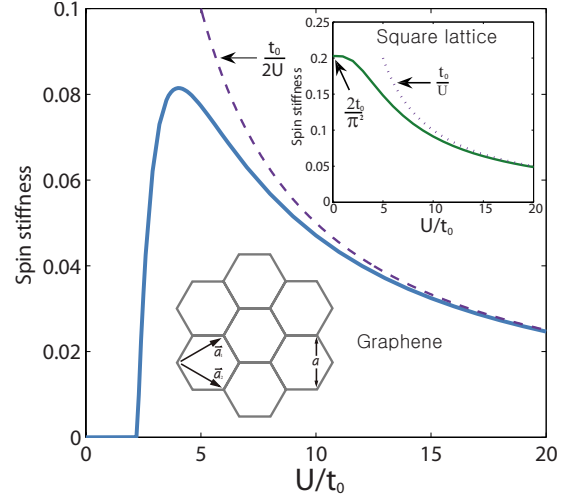


FIG. 1. (Color online) The spin stiffness of graphene as a function of U/t_0 at zero temperature. The spin stiffness is made to be dimensionless by dividing it with t_0 and a^2 . At $U/t_0 \approx 2.3$ where the local magnetic moment goes to zero, the spin stiffness vanishes. The dashed line corresponds to the classical limit of the Heisenberg model. Inset shows the stiffness curve for square lattice.

$$\begin{aligned} \rho_s = & \frac{t_0}{N} \sum_{\vec{k}} \left[- \frac{\beta}{4 \cosh^2 \frac{\beta \epsilon(\vec{k})}{2}} \left\{ \frac{\left(\frac{\partial |\phi|^2}{\partial k_y} \right)^2 + 2 \left| \Gamma \frac{\partial \phi}{\partial k_y} \right|^2}{\epsilon(\vec{k})^2} \right\} \right. \\ & \left. + \left\{ \frac{-\frac{\partial^2 |\phi|^2}{\partial k_y^2}}{2\epsilon(\vec{k})} + \frac{\left(\frac{\partial |\phi|^2}{\partial k_y} \right)^2 + 2 \left| \Gamma \frac{\partial \phi}{\partial k_y} \right|^2}{4\epsilon(\vec{k})^3} \right\} \tanh \frac{\beta \epsilon(\vec{k})}{2} \right], \end{aligned} \quad (6)$$

where $\epsilon(\vec{k}) = \sqrt{|\Gamma|^2 + |\phi|^2}$. Here we introduced dimensionless quantities such as $U \rightarrow U/t_0$ and $\beta \rightarrow t_0/k_B T$. We plot the spin stiffness as a function of on-site Coulomb repulsion U/t_0 at zero temperature in Fig. 1. In the limit of large U/t_0 , the spin stiffness approaches that of the classical Heisenberg model on graphene. When $U/t_0 \approx 2.3$, the spin stiffness vanishes because the antiferromagnetic order disappears exactly at the same point. This behavior is quite different from that of the square lattice whose spin stiffness goes immediately to a finite value $2t_0/\pi^2$ although its magnetic moments are infinitesimally small.⁴⁰ This stems from the different mechanisms for the formation of the magnetic order in the two cases. In case of the square lattice, its antiferromagnetic ground state originates from the Fermi-surface nesting at half filling. In contrast, graphene has no such large instability and the gap opening by the Neel order is only a perturbative process.

III. SPIN STIFFNESS OF THE ZIGZAG GRAPHENE NANORIBBON

We now consider the spin excitations of the graphene nanoribbon with zigzag edges. The ZGNR is illustrated in Fig.

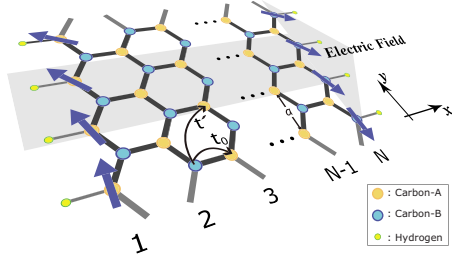


FIG. 2. (Color online) The hydrogen-passivated graphene nanoribbon with width N . It has translational symmetry along y axis and the lateral electric field is directed along x axis. The sublattices are represented by two different colors (yellow and blue). We consider at most two hopping processes, the nearest (t_0) and next-nearest (t') neighbor hoppings.

2 whose width is defined by the number of dimer lines of the ribbon. When graphene has zigzag boundaries, it has been shown that edge localized states exist near the band center.¹⁰ While these edge states prefer magnetic phase at any nonzero U/t_0 , the bipartite nature of the ZGNR choose an antiferromagnetic configuration between two edges. So we can consider spin excitations at all finite values of U/t_0 including the physical one $U/t_0 \approx 1$ at which 2D graphene is paramagnetic.¹¹

A. Hartree-Fock approximation for the ZGNR

We consider a ZGNR with hydrogen-passivated edges including the next-nearest-neighbor (nnn) hopping parameters in Fig. 2. The next-nearest-neighbor hopping processes break the particle hole symmetry and the charge neutrality at each carbon atom is also broken. So we should add off-site Coulomb interactions to the original Hubbard Hamiltonian. Although this additional Coulomb potential is negligible because of the small extra charge, it becomes important when the external electric field is applied on the ZGNR. For these reasons, the Hartree-Fock Hamiltonian for the ZGNR is given by

$$\mathcal{H}_{HF} = \mathcal{H}_0 + \mathcal{H}_{CI} + \mathcal{H}_{EF} + E_0, \quad (7)$$

where \mathcal{H}_0 is the kinetic part including up to the next-nearest-neighbor hopping terms, \mathcal{H}_{CI} is the long-range part of Coulomb-interaction Hamiltonian and \mathcal{H}_{EF} is from the lateral electric field. The ratio between the nearest (t_0) and next-nearest (t') tight-binding hopping parameters is $t'/t_0 \approx 0.2$.^{2,41,42} The Coulomb interaction consists of

$$\begin{aligned} \mathcal{H}_{CI} = & U \sum_{\sigma} \sum_{i,n} \sum_{\alpha} (\langle n_{(n,i),-\sigma}^{\alpha} \rangle n_{(n,i),\sigma}^{\alpha} - \sum_{i,n} \sum_{\alpha} (\Gamma_{(n,i)}^{\alpha} S_{(n,i)}^{\alpha+} \\ & + \Gamma_{(n,i)}^{\alpha*} S_{(n,i)}^{\alpha-}) + \sum_{i,j,n,m} \sum_{\alpha,\beta} \frac{e^2 \langle \Delta n_i^{\alpha} \rangle \cdot (1 - n_{(m,j)}^{\beta})}{4\pi\epsilon |\vec{r}_{n,i}^{\alpha} - \vec{r}_{m,j}^{\beta}|}, \end{aligned} \quad (8)$$

where the indices α and β are for the sublattice, n and m for the dimer line, i and j for the primitive cell and σ for the spin. The coefficient $\Gamma_{(n,i)}^{\alpha}$ of the interspin interaction is assumed to be

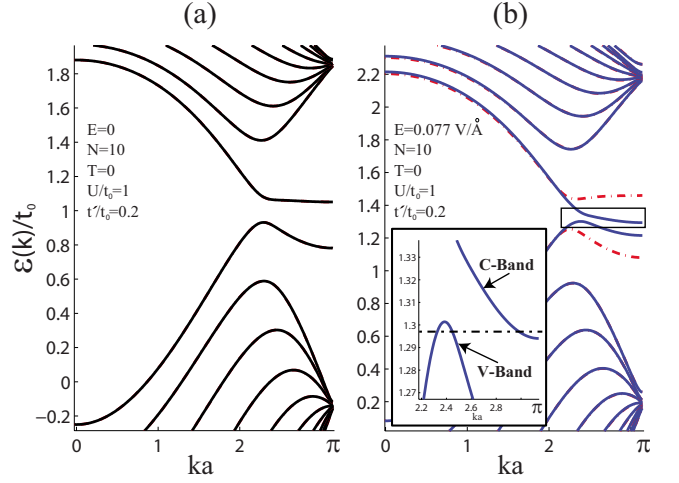


FIG. 3. (Color online) Band structures of graphene nanoribbon with width $N=10$ including the nnn hopping process. (a) Dispersion relations when there is no external field. (b) Transverse electric field (0.077 V/\AA) is applied to the GNR. The dispersion relation is spin dependent, which is indicated by two different colors (red and blue). The band structure near the Fermi level is depicted in the inset. Bands with a single species of spin are crossing the Fermi level and this is the realization of the half metallicity.

$$\Gamma_{(n,i)}^{\alpha} = U \langle S_{(n,i)}^{\alpha-} \rangle = \alpha \Gamma_i^{\alpha} e^{i\vec{q} \cdot \vec{r}_{(n,i)}^{\alpha}}, \quad (9)$$

where Γ_i^{α} is a positive constant and α multiplied to Γ_i^{α} stands for the antiferromagnetic coupling between two sublattices. In the last sum, \sum' means the sum is over different sites and $\langle \Delta n_i^{\alpha} \rangle \equiv 1 - \langle n_{(n,i),\uparrow}^{\alpha} \rangle - \langle n_{(n,i),\downarrow}^{\alpha} \rangle$. We suppose that the ZGNR is mounted on a SiO_2 substrate so that the dielectric constant ϵ is about 2.5.⁴³ \mathcal{H}_{EF} , the interaction with the external electric field is given by $\mathcal{H}_{EF} = \sum_{\sigma,\alpha} \sum_{i,n} e E x_i^{\alpha} n_{(n,i),\sigma}^{\alpha}$ where E is the strength of the electric field which is applied on the ZGNR along x axis. Finally, the constant E_0 is

$$E_0 = -U \sum_{i,n,\alpha} \langle n_{(n,i),\downarrow}^{\alpha} \rangle \langle n_{(n,i),\uparrow}^{\alpha} \rangle + \frac{1}{U} \sum_{i,n,\alpha} |\Gamma_{(n,i)}^{\alpha}|^2. \quad (10)$$

From this Hartree-Fock Hamiltonian, we calculate the spin stiffness of the ZGNR along the direction of the translational symmetry. We want to check whether our tight-binding model produces the results consistent with those from different methods. First, we consider the band structures of the ZGNR with width 10. When there is no Coulomb interaction, the ZGNR has nearly flat bands at the band center. Turning on the onsite Coulomb repulsion, The ZGNR prefers opening a gap by breaking the balance of spin occupation between two sublattices as shown in Fig. 3. Including the next-nearest hopping process (t'), the broken particle-hole symmetry opens an indirect gap which has a comparable size and shape with the previous first-principles calculation obtained by Son *et al.*^{7,9} When the transverse electric field is applied to the ribbon, we also note the gap closing of one spin species while the other one shows the gap opening as they have demonstrated. The critical electric field where the gap vanishes is found to be 0.054 V/\AA on the SiO_2 substrate as shown in Fig. 3 which is quite comparable with the discrete

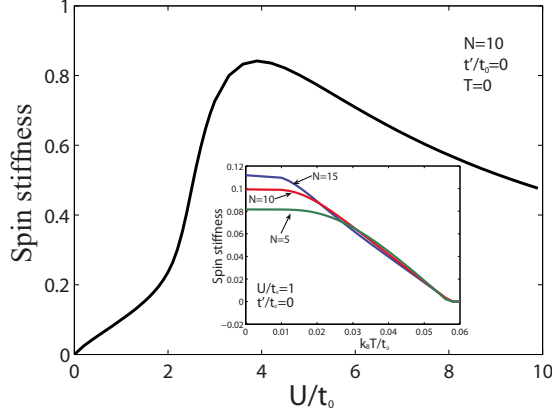


FIG. 4. (Color online) The spin stiffness of the GNR with width $N=10$ is plotted as a function of U/t_0 at zero temperature. Inset shows the temperature dependence of the spin stiffness of the GNR with various widths.

Fourier transform (DFT) calculation.^{9,44} Second, we also compare our spin stiffness with that from the first-principles calculations by Yazyev *et al.*²² Using the tight-binding model with the following choice of parameters $t_0=U=2.7$ eV, $t'=0.2t_0$ and the lattice constant $a=2.46$ Å, we have obtained $\rho_s \approx 1273$ meV Å² including both edges, while they found $\rho_s \approx 640$ meV Å² for single edge showing an excellent agreement between the two results.

U dependence of the ZGNR with width 10 is plotted in Fig. 4. Since we always consider the total energy per unit cell, we can compare the result in Fig. 4 with that of graphene by multiplying 10 to graphene's stiffness. From this, we notice that the stiffness is a bulk property at large U and a edge property at small $U (< 3t_0)$.

The temperature dependence of the ZGNR's spin stiffness with various widths is also studied and the results are shown in the inset of the Fig. 4.⁴⁵ One can notice that the thermal-fluctuation effects are almost negligible and the spin stiffness at room temperature ($k_B T \approx 0.01t_0$) remains almost the same as that at the zero temperature.

B. Spin stiffness of the ZGNR under the lateral electric field

As we have shown in the previous section, the gap of the ZGNR can be controlled by applying the lateral electric field and finally becomes half metallic above a certain critical value of electric field.⁹ This suggests a ZGNR to be potentially useful as a novel spintronics device. In the previous DFT study, it was found that the spin-correlation length of ZGNR is on the order of nanometer near room temperature. In spite of the lack of the magnetic anisotropy of the ZGNR, it has demonstrated a long spin-correlation length comparable to the other transition-metal chain system due to its high spin stiffness. Hence it will be worthwhile to obtain the spin stiffness of the ZGNR under the transverse electric field and check whether it maintains its high stiffness values even within the half-metallic phase.

Since the stiffness is shown to be robust against thermal fluctuations up to room temperature in the previous section, we only consider the zero-temperature behavior of the spin

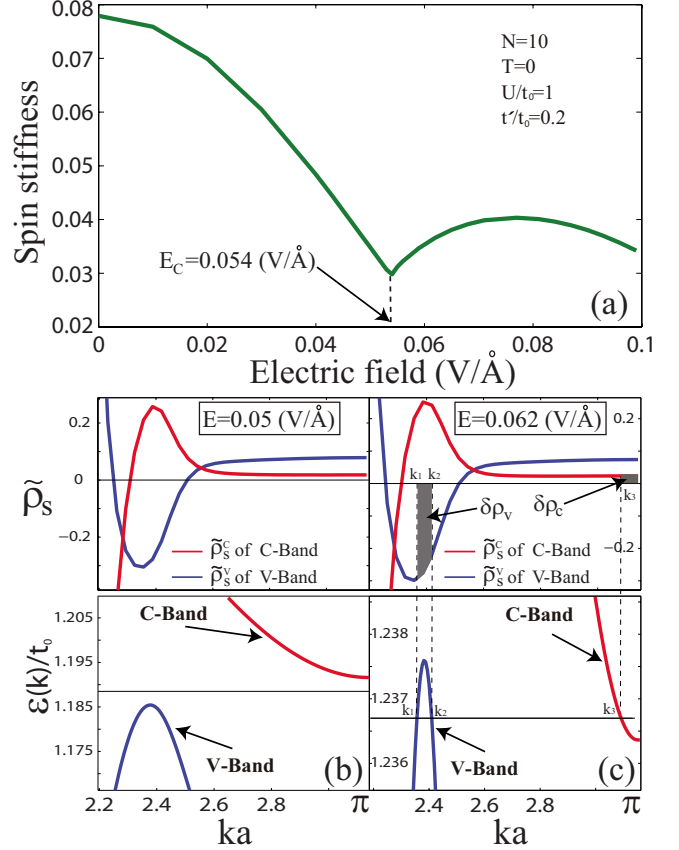


FIG. 5. (Color online) (a) Spin stiffness of GNR is depicted as a function of the transverse electric field. The GNR with ten dimer lines is considered at zero temperature. The typical experimental values of the on-site Coulomb repulsion and hopping parameters are chosen. At the critical electric field E_c , the spin stiffness curve shows a cusp. [(b) and (c)] Compare two different phases, below and above E_c . The upper panels of (b) and (c) are the k -resolved spin stiffness and the lower ones are the band structure near the Fermi level like the inset of Fig. 3(b). The red (blue) line is the k -resolved spin stiffness of the C band (V band) where C band (V band) is the nearest conduction (valence) band to the Fermi level.

stiffness. The results are shown in Fig. 5. Here, we assumed that the ZGNR with width 10 is on a silicon-oxide substrate and $t'=0.2t_0=0.2U$. As the electric field grows, the spin stiffness decreases and reaches less than half of that at zero electric field. However, there exists a critical electric field where the stiffness curve shows a cusp-like behavior and starts to increase. Then, the stiffness arrives at its maximum point in the half-metallic region and keeps decreasing again.

We notice that the cusp of the stiffness curve occurs at the insulator-metal transition point ($E \approx 0.054$ V/Å). We can explain this observation by introducing a k -resolved spin stiffness $\tilde{\rho}_s^i(k)$ which satisfies $\rho_s = \sum_n \int_{-\pi}^{\pi} \tilde{\rho}_s^i(k) dk$. This quantity explains how a state with k of the n th band contributes to the spin stiffness ρ_s . This is plotted in the upper panels of Figs. 5(a) and 5(b). Before the system enters into the half-metallic phase, the C band is empty so that no contributions from $\tilde{\rho}_s^c(k)$. After the insulator-metal transition occurs, however, the states between k_1 and k_2 are unoccupied while the states of C band from k_3 to the zone boundary can newly

participate. This kind of behavior contributes to the increase in the spin stiffness in two ways. One is by removing the states with negative $\tilde{\rho}$ from the V band which corresponds to $\delta\rho_V$ in the upper window of Fig. 5(c). Then electrons from this V -band transfer to more edge-localized states (near the zone boundary) of the C band which corresponds to $\delta\rho_C$. Since the k -resolved spin stiffness near the zone boundary is always positive, this transfer gains another positive contribution to the spin stiffness. In summary, as the electric field closes the band gap, electrons transfer from negative- $\tilde{\rho}$ states to the positive- $\tilde{\rho}$ states near the zone boundary and this is the reason why the spin stiffness starts to increase at the insulator-metal transition point.

IV. CONCLUSION

We have studied the spin stiffness of graphene and ZGNR based on the Hubbard model within the Hartree-Fock approximation. For both materials, the on-site U dependence of the spin stiffness has been investigated. Unlikely from the 2D graphene, which remains to be nonmagnetic at the presence of experimental value of Coulomb repulsion, the ZGNR acquires an edge magnetism. By analyzing the temperature dependence of the spin stiffness of ZGNR, we notice that the thermal-fluctuation effect on the spin stiffness is almost negligible up to the room temperature. We have also investigated

the effects of the external electric field applied laterally to the ZGNR on the spin stiffness. While the electric field reduces the spin stiffness significantly, we interestingly notice that the stiffness starts to increase above a certain critical electric field at which the half-metallicity sets in. For the finite temperature spintronics operation of the ZGNR, it will be quite important to increase the spin-stiffness value. Considering the U dependence of the ZGNR's spin stiffness, we note that the stiffness is monotonically increasing function of U until $U < 3t$. This means that the stretching or compressing the ZGNR can modify the spin stiffness of the ZGNR. Hence the strain may provide a room to improve the ZGNR's spin stiffness.^{46,47} Finally, it is important to understand how defects on GNRs may affect the spin stiffness. The effect of edge defects and impurities on the edge magnetism of ZGNRs has been previously studied by several groups.^{9,22,48} It has been known that various qualitative behaviors of edge magnetic states are maintained as long as defects do not damage the bipartite nature of both edges of the ZGNR substantially. Hence we expect that the above defects would not alter our results qualitatively.

ACKNOWLEDGMENT

This work was supported by the Korea Research Foundation Grant funded by the Korean Government (KRF-2008-313-C00243)

-
- ¹K. S. Novoselov, A. K. Geim, S. V. Morozov, D. Jiang, Y. Zhang, S. V. Dubonos, I. V. Grigorieva, and A. A. Firsov, *Science* **306**, 666 (2004).
- ²A. H. Castro Neto, F. Guinea, N. M. R. Peres, K. S. Novoselov, and A. K. Geim, *Rev. Mod. Phys.* **81**, 109 (2009).
- ³A. K. Geim and K. S. Novoselov, *Nature Mater.* **6**, 183 (2007).
- ⁴P. Esquinazi, A. Setzer, R. Höhne, C. Semmelhack, Y. Kopelevich, D. Spemann, T. Butz, B. Kohlstrunk, and M. Lösche, *Phys. Rev. B* **66**, 024429 (2002).
- ⁵P. Esquinazi, D. Spemann, R. Höhne, A. Setzer, K.-H. Han, and T. Butz, *Phys. Rev. Lett.* **91**, 227201 (2003).
- ⁶O. V. Yazyev, *Phys. Rev. Lett.* **101**, 037203 (2008).
- ⁷Y.-W. Son, M. L. Cohen, and S. G. Louie, *Phys. Rev. Lett.* **97**, 216803 (2006).
- ⁸Li Yang, C.-H. Park, Y.-W. Son, M. L. Cohen, and S. G. Louie, *Phys. Rev. Lett.* **99**, 186801 (2007).
- ⁹Y.-W. Son, M. L. Cohen, and S. G. Louie, *Nature (London)* **444**, 347 (2006).
- ¹⁰M. Fujita, K. Wakabayashi, K. Nakada, and K. Kusakabe, *J. Phys. Soc. Jpn.* **65**, 1920 (1996).
- ¹¹L. Pisani, J. A. Chan, B. Montanari, and N. M. Harrison, *Phys. Rev. B* **75**, 064418 (2007).
- ¹²C. Jozsa, M. Popinciuc, N. Tombros, H. T. Jonkman, and B. J. van Wees, *Phys. Rev. B* **79**, 081402(R) (2009).
- ¹³Blanca Biel, X. Blase, Francois Triozon, and Stephan Roche, *Phys. Rev. Lett.* **102**, 096803 (2009).
- ¹⁴S. Dutta, A. K. Manna, and S. K. Pati, *Phys. Rev. Lett.* **102**, 096601 (2009).
- ¹⁵J. Nakabayashi, D. Yamamoto, and S. Kurihara, *Phys. Rev. Lett.* **102**, 066803 (2009).
- ¹⁶Z. Li, H. Qian, J. Wu, B.-L. Gu, and W. Duan, *Phys. Rev. Lett.* **100**, 206802 (2008).
- ¹⁷M. Wimmer, İ. Adagideli, S. Berber, D. Tomanek, and K. Richter, *Phys. Rev. Lett.* **100**, 177207 (2008).
- ¹⁸T. Fang, A. Konar, H. Xing, and D. Jena, *Phys. Rev. B* **78**, 205403 (2008).
- ¹⁹Hengyi Xu, T. Heinzl, M. Ewaldsson and I. V. Zozoulenko, *Phys. Rev. B* **77**, 245401 (2008).
- ²⁰J. Jung, T. Pereg-Barnea, and A. H. MacDonald, *Phys. Rev. Lett.* **102**, 227205 (2009).
- ²¹D. A. Areshkin and B. K. Nikolić, *Phys. Rev. B* **79**, 205430 (2009).
- ²²O. V. Yazyev and M. I. Katsnelson, *Phys. Rev. Lett.* **100**, 047209 (2008).
- ²³L. Jiao, X. W. Li Zhang, G. Diankov, and H. Dai, *Nature (London)* **458**, 877 (2009).
- ²⁴Dmitry V. Kosynkin, Amanda L. Higginbotham, Alexander Sinitskii, Jay R. Lomeda, Ayrat Dimiev, B. Katherine Price, and James M. Tour, *Nature (London)* **458**, 872 (2009).
- ²⁵X. Jia, M. Hofmann, V. Meunier, B. G. Sumpter, J. Campos-Delgado, J. M. Romo-Herrera, H. Son, Y.-P. Hsieh, A. Reina, J. Kong, M. Terrones, and M. S. Dresselhaus, *Science* **323**, 1701 (2009).
- ²⁶Jessica Campos-Delgado, Jos Manuel Romo-Herrera, Xiaoting Jia, David A. Cullen, Hiroyuki Muramatsu, Yoong Ahm Kim, Takuya Hayashi, Zhifeng Ren, David J. Smith, Yu Okuno, To-

- monori Ohba, Hirofumi Kanoh, Katsumi Kaneko, Morinobu Endo, Humberto Terrones, Mildred S. Dresselhaus, and Mauricio Terrones, *Nano Lett.* **8**, 2773 (2008).
- ²⁷X. Li, X. Wang, S. L. Li Zhang, and H. Dai, *Science* **319**, 1229 (2008).
- ²⁸L. Tapaszto, G. Dobrik, P. Lambin, and L. P. Biro, *Nat. Nanotechnol.* **3**, 397 (2008).
- ²⁹K. A. Ritter and J. W. Lyding, *Nature Mater.* **8**, 235 (2009).
- ³⁰X. Wang, Y. Ouyang, X. Li, H. Wang, J. Guo, and H. Dai, *Phys. Rev. Lett.* **100**, 206803 (2008).
- ³¹C. Stampfer, J. Guttinger, S. Hellmuller, F. Molitor, K. Ensslin, and T. Ihn, *Phys. Rev. Lett.* **102**, 056403 (2009).
- ³²M. Y. Han, B. Ozyilmaz, Y. Zhang, and P. Kim, *Phys. Rev. Lett.* **98**, 206805 (2007).
- ³³Yu-Ming Lin, Vasili Perebeinos, Zhihong Chen, and Phaedon Avouris, *Phys. Rev. B* **78**, 161409(R) (2008).
- ³⁴E. H. Lieb, *Phys. Rev. Lett.* **62**, 1201 (1989).
- ³⁵B. I. Halperin and P. C. Hohenberg, *Phys. Rev.* **188**, 898 (1969).
- ³⁶J. M. J. van Leeuwen, M. S. L. du Croo de Jongh, and P. J. H. Denteneer, *J. Phys. A* **29**, 41 (1996).
- ³⁷P. J. H. Denteneer, Guozhong An, and J. M. J. van Leeuwen, *Phys. Rev. B* **47**, 6256 (1993).
- ³⁸Z.-P. Shi and R. R. P. Singh, *Europhys. Lett.* **31**, 219 (1995).
- ³⁹N. M. R. Peres, M. A. N. Araujo and Daniel Bozi, *Phys. Rev. B* **70**, 195122 (2004).
- ⁴⁰P. Kopietz, *Z. Naturforsch. B* **89**, 351 (1992).
- ⁴¹S. Reich, J. Maultzsch, C. Thomsen, and P. Ordejón, *Phys. Rev. B* **66**, 035412 (2002).
- ⁴²The value of t' is known to have quite wide range of uncertainty ($0.02t_0 < t' < 0.2t_0$) depending on the parametrization schemes (Ref. 41). We note that as t' increases from zero to $0.2t_0$, the spin stiffness decreases to about 80% of its value at $t'=0$, while the qualitative behavior of the spin stiffness as a function of Coulomb repulsion, temperature, and the electric field remains unchanged.
- ⁴³E. H. Hwang and S. Das Sarma, *Phys. Rev. B* **75**, 205418 (2007).
- ⁴⁴We also evaluated the critical field for the suspended ZGNR ($E_c \approx 0.093$ V/Å) while Son *et al.* obtained $E_c \approx 0.14$ V/Å for the ZGNR with width 11.
- ⁴⁵As the ribbon width increases, the spin stiffness increases in spite of the decay of the coupling between two ferromagnetic edges. This is due to our definition of spin stiffness based on the total energy per unit cell *not* per edge C atom. This kind of width dependence is also shown in Ref. 11.
- ⁴⁶F. Liu, P. Ming, and J. Li, *Phys. Rev. B* **76**, 064120 (2007).
- ⁴⁷K. S. Kim, Y. Zhao, H. Jang, S. Y. Lee, J. M. Kim, K. S. Kim, J.-H. Ahn, P. Kim, J.-Y. Choi, and B. H. Hong, *Nature (London)* **457**, 706 (2009).
- ⁴⁸B. Huang, F. Liu, J. Wu, B.-L. Gu, and W. Duan, *Phys. Rev. B* **77**, 153411 (2008).